JOURNAL OF CATALYSIS 157, 740–748 (1995)

The Effect of Acid–Base Properties of Supported Molybdenum Oxide in Propylene Oxidation

Anantha N. Desikan, Weimin Zhang, and S. Ted. Oyama[1]

Department of Chemical Engineering, Virginia Polytechnic Institute and State University, Blacksburg, Virginia 24061-0211

Received June 6, 1995; revised August 18, 1995; accepted August 21, 1995

Samples of molybdenum oxide supported on SiO_2, Al_2O_3, and TiO_2 were used to study the effect of loading and support on propylene oxidation. The samples were characterized by oxygen chemisorption, temperature programmed reduction (TPR), and temperature programmed surface reaction (TPSR) of adsorbed ethanol. Oxygen chemisorption and TPR results indicated that the molybdenum oxide–support interaction increased in the order $SiO_2 < Al_2O_3 < TiO_2$. TPSR of adsorbed ethanol was used to characterize the acid–base properties of the catalysts. These properties played an important role in the surface reactions of the highly dispersed low-loading samples and resulted in the formation of oxidation products depending on the supports (acrolein on MoO_3/SiO_2, acetaldehyde on MoO_3/Al_2O_3, and acetone on MoO_3/TiO_2). In higher loading samples these differences were reduced as support effects became less important.

INTRODUCTION

Molybdenum oxide is a principal component in catalysts for the selective oxidation and ammoxidation of propylene as well as many other catalysts of industrial importance (1–5). Characterization and reactivity studies of these catalysts have been the topic of numerous investigations (6–13). To understand the role of molybdenum oxide in these multicomponent catalysts, a number of studies on propylene oxidation over unsupported and supported molybdenum oxide have been performed (14–19). The main body of literature on propylene oxidation over molybdenum oxide, however, lacks a thorough study of the effect of catalyst support. It is known that the surface properties of molybdenum oxide are strongly influenced by the type of oxide support and result in different catalytic activity (6–10, 20). The lack of systematic studies with well-characterized samples (surface area, acidity, basicity) has made it difficult to compare activity on different supports. In this investigation we employ the results of a recently developed method for counting surface sites on unsupported and supported molybdenum oxide to obtain turnover rates for propylene oxidation and to study the effect of support on the activity. We show that acid–base interactions of the molybdenum oxide with the support affects not only the structure and properties of the surface species, but also their catalytic reactivity and selectivity.

The importance of molybdenum oxide catalysts in catalytic applications has prompted a large number of studies concerning the surface structures and the effect of the oxide support on the surface properties using various spectroscopic techniques such as ultraviolet–visible spectroscopy (UV–Vis) (21—24), infrared spectroscopy (IR) (22, 25—27), electron spin resonance spectroscopy (ESR) (28–30), ion scattering spectroscopy (ISS) (31, 32), X-ray photoelectron spectroscopy (XPS) (31, 32), and laser Raman spectroscopy (32–39). There is increasing evidence that the acid–base properties of the support influence the surface structures and the level of interaction of the support with molybdenum oxide (9, 10, 40, 41).

Surface acidity and basicity measurements on oxide catalysts have received considerable attention in recent years since they play an important role in the selective oxidation of hydrocarbons (42–44). Catalytic activity has been closely related to the acidity and basicity of binary oxides (45, 46). The acidic properties of multicomponent metal oxides are generally determined by means of appropriate probe molecules acting as titrants or adsorbents (44, 47). In this paper we utilize the temperature programmed surface reaction (TPSR) of ethanol as a method for determining the acid–base properties of MoO_3 supported on SiO_2, Al_2O_3, and TiO_2. The effect of the acid–base properties of these supported molybdenum oxide samples on the propylene oxidation reaction will be presented.

EXPERIMENTAL

Gases used in these studies were helium (Linde Ultra High Purity Grade 99.999%), hydrogen (Linde Ultra High Purity Grade 99.999%), oxygen (Linde Ultra High Purity Extra Dry Grade 99.6%), nitrogen (Linde Ultra High Purity Grade 99.999%), carbon monoxide (Linde Research

[1] To whom correspondence should be addressed.

0021-9517/95 $12.00

Grade 99.97%), and propylene (Linde 99.0%). The liquids used were research grade dehydrated ethanol (Pharmco 99%), acetaldehyde (Aldrich 99%), and diethyl ether (Mallinckrodt).

Supported MoO_3 catalysts were prepared by impregnating SiO_2 (Cabosil L90, SA 90 $m^2\ g^{-1}$), Al_2O_3 (Degussa Aluminumoxid C, SA 100 $m^2\ g^{-1}$), and TiO_2 (Degussa P25, SA 50 $m^2\ g^{-1}$) with solutions of ammonium molybdate (Aldrich 98%) in distilled water to the point of incipient wetness. These materials were then dried at 393 K for 6 h and calcined at 773 K for 6 h.

Oxygen chemisorption, surface area, reactivity, temperature programmed desorption (TPD), temperature programmed reduction (TPR), and temperature programmed surface reaction experiments were measured in a flow apparatus equipped with a computer-interfaced mass spectrometer (Dycor/Ametek Model MA 100). For the oxygen uptake measurements, 0.5-g samples were oxidized in air at 773 K and then reduced in flowing 50-mol% H_2/He mixtures for 2 h at various temperatures. Uptakes were determined at the same temperature by injecting 10 μmol pulses of oxygen from a calibrated on-line sampling valve onto a He stream passing over the reduced samples. Surface areas were determined by the conventional single-point BET method. The measurements were made by flowing a 30-mol% N_2/He mixture over samples held at liquid N_2 temperatures and subsequently flashing off the adsorbed amount.

Catalytic activity was obtained in a 15-mm o.d./13-mm i.d. quartz packed-bed flow reactor at a total flow rate of 70–71 μmol s^{-1} and a total pressure of 101 kPa. (Flow rates in μmol s^{-1} may be converted to cm^3 (NTP) min^{-1} by multiplying by 1.5.) In the reactivity experiments the partial pressure of the reactants were $P_{C_3H_6}$ = 10 kPa, P_{O_2} = 10 kPa, P_{H_2O} = 5 kPa, and P_{He} = 75.1 kPa. In all the experiments amounts of catalyst corresponding to 21 μmol of O_2 uptake were loaded in the reactor. Particular care was used to ensure that the catalysts were stable under the reaction conditions employed. Before every run the catalysts were pretreated in the O_2–He–H_2O mixture (without C_3H_6) for 1 h at the maximum temperature of reaction. During the reactivity measurements, after the highest temperature was attained, a lower temperature measurement was always repeated to verify catalyst stability and lack of deactivation. To further check for any changes in the properties of the catalyst during reaction, oxygen chemisorption and surface area measurements were performed on the catalysts after reactivity measurements. For analysis of the reactants and products a multiple linear least square regression technique was used to account for the fragmentation of the different components. Mass fragmentation patterns and the relative abundance of the relevant compounds were determined by performing independent calibration experiments. Carbon balances closed to 100 ± 10%. Rates are reported as turnover rates based on the surface molybdenum atoms counted by chemisorbed oxygen atoms.

$$v_t = \frac{Qyx}{Vw2S}$$

In the equation above, v_t is the total propylene turnover rate, Q is the total volumetric flow rate, y is the mole fraction of propylene, V is the molar volume at the condition of flow measurement, w is the weight of the catalyst, and S is the molecular oxygen uptake value.

TPR experiments employed a 5% H_2/He mixture (33.3 μmol s^{-1}), a linear heating rate of 0.17 K s^{-1}, a standard pretreatment in air at 773 K for 3600 s, followed by a He purge, and a final isothermal heating period of 1800 s. A desiccant bed (Drierite, $CaSO_4$) removed the water produced during reduction and the hydrogen consumption was recorded in the form of negative peaks. For the ethanol TPSR studies, ethanol was adsorbed at 298 K for 3600 s, by passing a continuous mixture of 10% ethanol/He over the catalyst calcined at 773 K for 3600 s. After the system was purged with He at 298 K for 3600 s, a flow of 33 μmol s^{-1} of He was established and the product distribution was followed by mass spectrometry as the temperature was ramped at 0.10 K s^{-1}. Again, independent calibrations were performed to determine the fragmentation patterns and relative abundance values of the different components formed during the surface reaction. The raw data was then analyzed by multiple linear least square regression to yield the amounts of the various compounds desorbed during the experiment.

RESULTS

Figure 1 shows the oxygen uptake values for SiO_2-, Al_2O_3-, and TiO_2-supported samples plotted versus the amount of molybdenum in the samples. The values in units of μmol m^{-2} account for the sample surface area. In all cases the uptake values increase with MoO_3 loading and at low loadings (1 wt% for SiO_2, 1–9 wt% for Al_2O_3, and 1–5 wt% for TiO_2) the uptake curves approach the dashed lines corresponding to complete dispersion, defined as a stoichiometry of one oxygen atom per molybdenum atom (O: Mo = 1). At high loadings (5–9 wt% for SiO_2, 12–20 wt% for Al_2O_3, and 5–9 wt% for TiO_2) the uptake curves deviate from the dashed lines indicating lower dispersions.

Figure 2 presents the TPR patterns of three low-loading supported samples and compares them with that of unsupported MoO_3. The appearance of the first reduction peak (T_{red}) indicated by arrows depends on the support material used with $T_{red} - TiO_2 < T_{red} - Al_2O_3 < T_{red} - SiO_2$. The other reduction peaks at higher temperature appear close

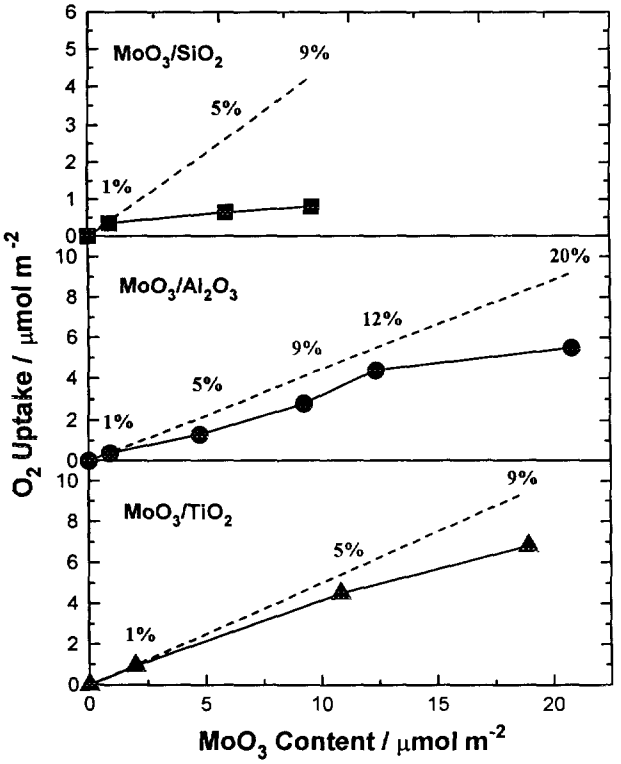

FIG. 1. Comparison of oxygen uptake values on supported MoO_3 catalysts.

to those of unsupported MoO_3 and correspond to reduction of Mo to a low oxidation state.

Figure 3 displays the ethanol TPSR traces on the pure supports. There is considerable desorption of ethanol (>40%) on all supports (SiO_2, 356 K; Al_2O_3, 378 K; and TiO_2, 361 K). All percentages reported in this paper are in mol% based on ethanol (CO and $CO_2 \div 2$, diethylether $\times 2$). On Al_2O_3 and TiO_2 ethylene desorbs at around 524 and 598 K and diethylether desorbs at around 462 and 555 K, respectively. On SiO_2 traces of the ethylene desorb at around 830 K. On TiO_2 traces of carbon oxides are produced at around 740 K.

Figure 4 compares the ethanol TPSR traces on the low-loading samples on the three different supports. Again on all the samples, there is considerable amount of ethanol desorption (>45%) with the T_{max} of desorption varying slightly with the support (MoO_3/SiO_2, 354 K; MoO_3/Al_2O_3, 371 K; and MoO_3/TiO_2, 363 K). The desorption characteristics of the other products differ considerably on the three samples. On the SiO_2-supported sample diethylether is not produced and ethylene desorbs at around 770 K. On the Al_2O_3-supported sample, diethylether and ethylene desorb at around 455 K and 500 K, respectively. On the TiO_2-supported sample diethylether, ethylene and carbon oxides desorb at around 530, 540, and 720 K, respectively.

Figure 5 presents the ethanol TPSR traces of the high-loading supported samples. As in the case of the low-loading samples, there is considerable ethanol desorption (>55%) with a slight variation of T_{max} of desorption (MoO_3/SiO_2, 353 K; MoO_3/Al_2O_3, 369 K; and MoO_3/TiO_2, 358 K). Acetaldehyde is produced in considerable amounts on all the samples (MoO_3/SiO_2, 15%; MoO_3/Al_2O_3, 39%; and MoO_3/TiO_2, 24%) and desorbs at around 410 K. Diethylether is also produced on all the samples (<10%) and desorbs at around 410 K (MoO_3/SiO_2), 420 K (MoO_3/Al_2O_3), and 400 K (MoO_3/TiO_2), respectively. In addition, carbon oxides are produced on the SiO_2 (670 K) and TiO_2 (710 K) supported samples and ethylene (748 K) is produced on the SiO_2 supported sample. Ethanol TPSR from medium-loading samples (5% MoO_3/TiO_2 and 9% MoO_3/Al_2O_3) were also measured, but these showed results very similar to those of the high-loading samples and the data for these are not presented here.

Figure 6 compares Arrhenius plots for propylene oxidation on the low-loading samples for the three different supports. The plots show that the turnover rates increase in the order $SiO_2 < Al_2O_3 < TiO_2$ while the activation energies decrease in the same order, 73, 67, and 52 kJ mol^{-1}.

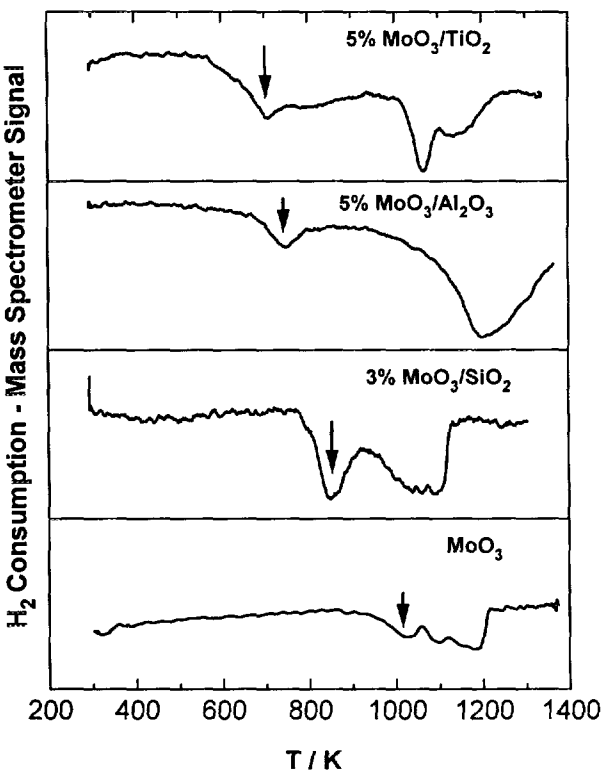

FIG. 2. Temperature programmed reduction traces of low-loading supported MoO_3 and unsupported MoO_3. Samples were reduced in 5 mol% H_2/He (33 μmol s^{-1}) as the temperature was ramped at 0.17 K s^{-1}. Prior to the TPR catalysts were calcined in O_2 at 773 K for 3600 s.

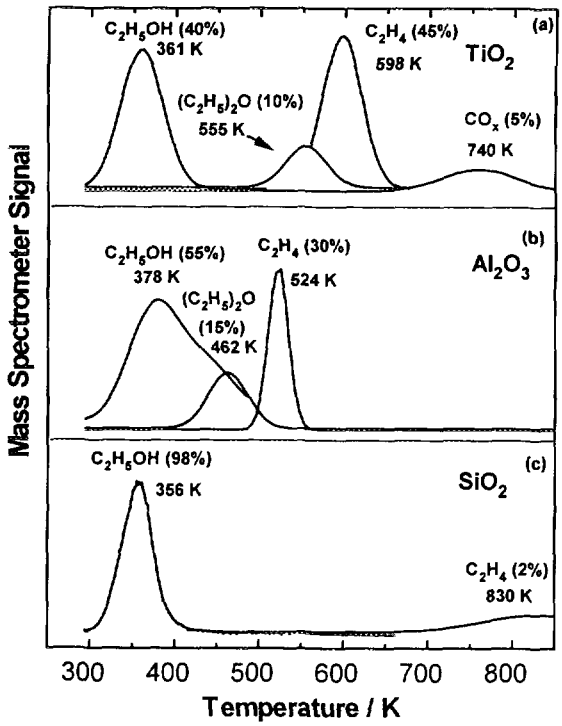

FIG. 3. Temperature programmed surface reaction of adsorbed ethanol on catalyst supports. Equivalent total ethanol adsorption is 0.50 μmol m^{-2} on TiO_2, 0.44 μmol m^{-2} on Al_2O_3 and 0.11 μmol m^{-2} on SiO_2.

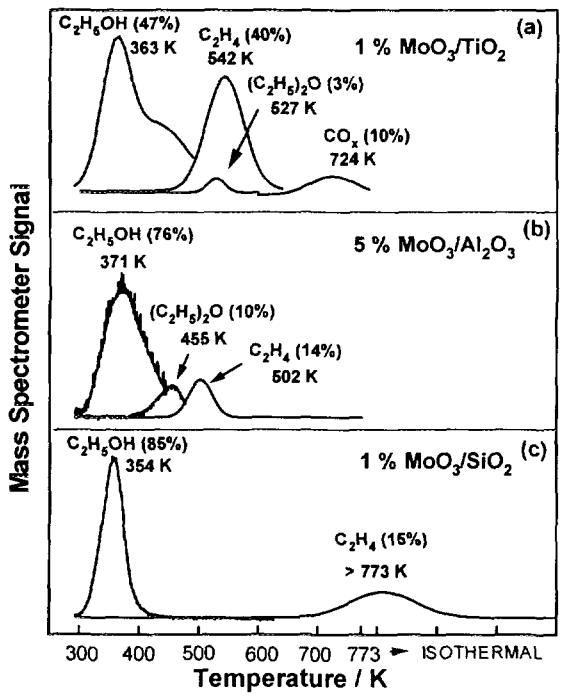

FIG. 4. Temperature programmed surface reaction of adsorbed ethanol on low-loading MoO_3 samples. Equivalent total ethanol adsorption is 0.60 μmol m^{-2} on MoO_3/TiO_2, 0.30 μmol m^{-2} on MoO_3/Al_2O_3 and 0.13 μmol m^{-2} on MoO_3/SiO_2.

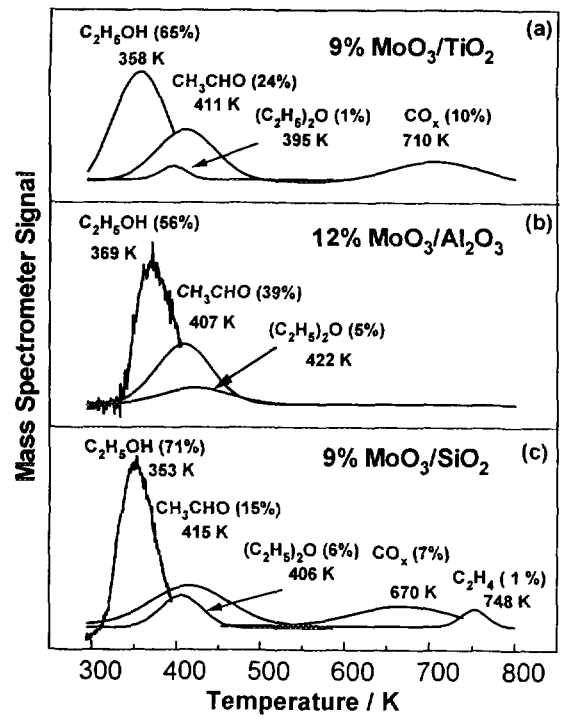

FIG. 5. Temperature programmed surface reaction of adsorbed ethanol on high-loading MoO_3 samples. Equivalent total ethanol adsorption is 0.66 μmol m^{-2} on MoO_3/TiO_2, 0.75 μmol m^{-2} on MoO_3/Al_2O_3 and 0.55 μmol m^{-2} on MoO_3/SiO_2.

The blank activity of the pure supports was completely negligible even at the highest temperatures reached in this study. Figure 7 displays the Arrhenius plots for propylene oxidation on the high-loading samples. On these samples the activity differences are largely leveled and the points fall on one line with activation energy 47 kJ mol^{-1}. The magnitudes of the rates are close to those of the low-loading samples.

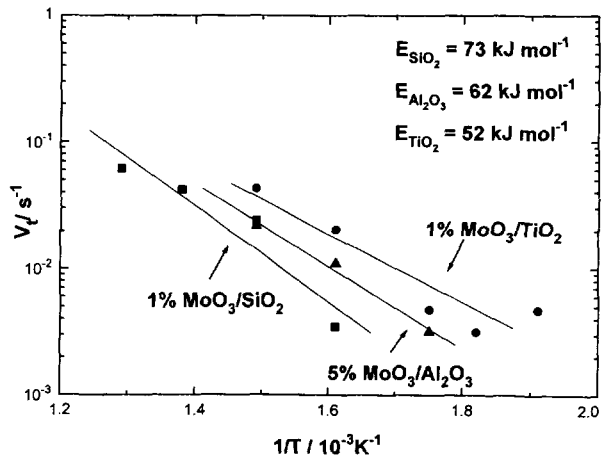

FIG. 6. Arrhenius plots for propylene oxidation on low-loading MoO_3 samples.

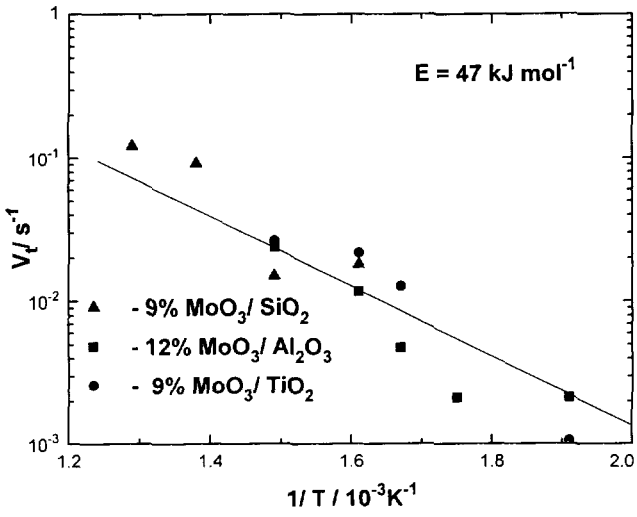

FIG. 7. Arrhenius plots for propylene oxidation on high-loading MoO_3 samples.

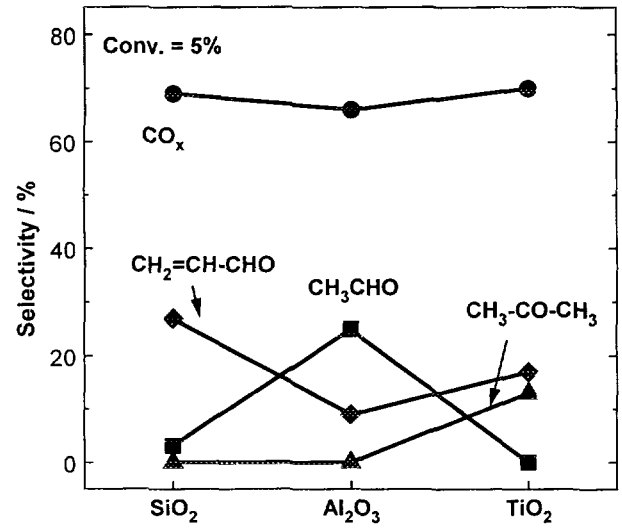

FIG. 9. Effect of catalyst support for high-loading MoO_3 samples on product selectivity in propylene oxidation.

Figure 8 compares the effect of support in the low-loading samples on the selectivity to different products for propylene oxidation made at similar conversions (<5%). There are considerable differences between the supports. On the SiO_2-supported sample, acrolein along with traces of propionaldehyde are the selective oxidation products. On the Al_2O_3-supported sample, acetaldehyde is the only selective oxidation product and on the TiO_2-supported sample, acetone is the only selective oxidation product. The selectivity to partial oxidation is ~30–40% on all the supported samples.

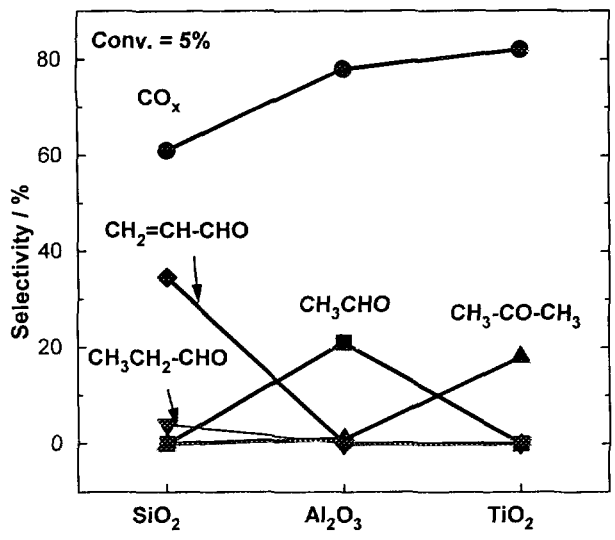

FIG. 8. Effect of catalyst support for low-loading MoO_3 samples on product selectivity in propylene oxidation.

Figure 9 shows the effect of support in the high-loading samples on the selectivity to different oxidation products for propylene oxidation again, at similar conversions (<5%). As with the activity, differences in selectivity are also leveled, and acrolein is produced on all samples. There is some residual effect of support and, similarly to the low-loading samples, some acetaldehyde is produced on the Al_2O_3-supported sample; acetone is produced on the TiO_2-supported sample. Selectivity to total oxidation products is ~30% on all the supported samples. Table 1 summarizes the values of conversion, turnover rates, and selectivities for all the supported samples.

DISCUSSION

Complete studies of oxygen chemisorption on unsupported and supported MoO_3 have been reported elsewhere (48, 49). In these studies, reduction and chemisorption temperatures were varied systematically to give results consistent with Raman spectroscopy at low loadings and X-ray diffraction at high loadings. Oxygen uptake values are compared for the SiO_2-, Al_2O_3-, and TiO_2-supported samples as a function of MoO_3 loading in Fig. 1. In the SiO_2 system, samples of 3 wt% loading and higher have oxygen uptake values that fall well beneath the dashed line corresponding to O/Mo = 1, indicating low dispersion. For the Al_2O_3- and TiO_2-supported samples the drop off occurs at loadings of 5 and 9 wt%, respectively. Allowing for differences in surface area, these values indicate that the order of interaction is $SiO_2 < Al_2O_3 \leq TiO_2$. Raman spectroscopy further shows that at high loadings on all supports molybdenum oxide is in the form of small crystallites with structures identical to bulk MoO_3 (36, 48–50).

TABLE 1

Propylene Oxidation on Supported MoO_3 Catalysts

Catalyst	T(K)	Selectivity (%)					Conversion (%)	υ_t (s^{-1})
		CH_3CHO	C_3H_6CHO	C_3H_4O	CH_3COCH_3	CO_x		
	623	—	5	35	—	60	4	0.0070
1.0% MoO_3/SiO_2	673	2	3	31	—	64	3	0.0050
	723	4	3	17	—	76	50	0.084
	623	3	—	28	—	69	11	0.018
9.0% MoO_3/SiO_2	673	—	8	28	—	64	9	0.015
	723	5	3	16	—	76	55	0.092
	573	20	—	—	2	78	1.9	0.0030
1.0% MoO_3/Al_2O_3	623	6	—	1	7	85	6.6	0.011
	573	25	—	6	—	66	1.2	0.0020
12.0% MoO_3/Al_2O_3	623	6	—	1	8	85	7.2	0.012
	573	—	—	—	18	82	2.8	0.0048
1.0% MoO_3/TiO_2	623	—	—	—	19	81	12.4	0.021
	673	—	—	—	6	94	25.7	0.043
	573	—	—	17	13	70	0.95	0.0016
9.0% MoO_3/TiO_2	623	8	—	9	8	77	14.3	0.023
	673	8	—	7	6	79	14.6	0.024

At low concentrations the supported molybdenum oxide consists of highly dispersed surface molybdate species containing a single molybdenum atom. The structure of the highly dispersed phase in the absence of water is probably an $O{=}MoO_4$ monomer with four bridging oxygen links to the surface. On silica this may hydrate to a dioxo form (48).

Temperature programmed reduction (Fig. 2) confirms the order of interaction to be $SiO_2 < Al_2O_3 < TiO_2$ as seen in the progression of T_{red} in the low-temperature reduction peak. The high-temperature reduction peaks for the alumina-supported sample occur at the highest temperature probably because of the strong interaction of MoO_2 with the support surface. All of these high-temperature reduction features are irrelevant to the work presented in this paper because they involve Mo in very low oxidation states. The first reduction peak alone occurs in the temperature range where reaction is observed.

Figures 3–5 summarize the temperature programmed desorption traces of ethanol on a series of supported samples and supports. On all samples, ethanol desorbs intact at relatively low temperatures (<380 K), while at higher temperatures, reaction products start to appear. On the supports (Fig. 3) and the low-loading TiO_2- and Al_2O_3-supported samples (Fig. 4), dehydration of ethanol to form diethylether and ethylene are the major reaction pathways. On the low-loading SiO_2 sample, a small amount of ethylene desorbs at very high temperatures. On the high-loading samples (Fig. 5), dehydrogenation of ethanol to acetaldehyde and dehydration to diethylether are the major channels.

At low loadings, MoO_3 is highly dispersed on the support and the desorption pathways are controlled to a certain extent by the properties of the support. As the loading increases the MoO_3 coverage increases and isolated crystallites of bulk MoO_3 appear. The desorption products on these samples are increasingly controlled by the properties of bulk MoO_3.

There are very few studies in the literature on the temperature programmed desorption of ethanol from molybdenum oxide catalysts. Sleight and co-workers studied the structural effects of alcohol chemisorption and temperature programmed desorption on unsupported MoO_3 catalysts (51). They found that at low temperatures (~373 K) ethanol desorbs intact and at higher temperatures as acetaldehyde. Dehydration occurred to a very minor extent. This agrees with our results for the high-loading samples which are more representative of the properties of unsupported MoO_3.

There has been considerable work in the area of methanol dehydration over oxide and zeolite catalysts (52–55). Various mechanisms have been proposed for the dehydration of methanol to dimethylether involving interactions with both surface acid and base sites. Padamanabhan and Eastburn have shown kinetic evidence for the dual site mechanism for ether formation from methanol involving acid–base pairs on an alumina catalyst (52). Selectivity in the decomposition reaction of isopropanol has long been

regarded as one of the typical reactions for investigating the acid–base properties of catalytic sites on metal oxides (56–59). The catalysts can be classified according to their propensity toward dehydration to propene or dehydrogenation to acetone. As in the case of methanol decomposition, the isopropanol decomposition involves an acid–base dual site mechanism (60, 61).

Sleight and co-workers also found on unsupported MoO_3 that the desorption characteristics of methanol, ethanol, and isopropanol were essentially the same (51). Thus the same acid–base mechanism found to apply for methanol desorption probably also applies to the ethanol reaction. Recently, Decanio *et al.* have studied the nature of acid–base sites on γ-alumina and fluorided alumina by using TPSR of [^{18}O]ethanol (62, 63). They concluded that surface bound alkoxides are formed by (a) dissociative adsorption on Lewis acid sites and (b) nucleophilic attack by the surface oxide on the alcohol. They also state that alkenes may be formed by the dehydration of alkoxides adsorbed on basic sites rather than the dehydration of adsorbed alcohol as suggested by Knözinger *et al.* (64). Their results also suggest that when the surface alkoxide population decreases, alkenes can form from the dehydration of adsorbed alkoxides on either of the two sites. Studies on MgO catalysts have shown that alkenes are formed with high selectivities via a base-catalyzed dehydration of alcohols (65). It has also been shown that on alumina, acid site strength distribution controls the selectivity to ether and olefin formation. Lower strength acid sites lead to the formation of ether while relatively strong acid sites promote olefin formation (66). Thus, in Figs. 3–5, ethanol is probing both the acid and base properties of the supported catalysts.

Although SiO_2 is almost inert for the production of diethylether and ethylene (Fig. 4c), on the low loading TiO_2- and Al_2O_3-supported samples considerable amounts of diethylether indicate the presence of a bifunctional surface supporting both acid and base sites (Figs. 4a and 4b). However, the acid–base site strength distribution is different for the two supports, with TiO_2-supported samples having more basic sites of higher strength as seen from the larger production of ethylene on these samples (40%, TiO_2; 14%, Al_2O_3). The T_{max} of ethylene desorption also varies considerably indicating the difference in the strength of the sites with TiO_2 (542 K) > Al_2O_3 (502 K). On the pure TiO_2 and Al_2O_3 supports (Figs. 3a and 3b) the acid–base site strength distribution is almost the same on both supports, sites on TiO_2 being slightly stronger. The same trend is followed for the T_{max} of ethylene desorption with TiO_2 (598 K) > Al_2O_3 (524 K). In contrast, the T_{max} for ethylene and diethylether desorption on the supports is higher than that for the low-loading samples. This difference may be caused by a decrease in the number of acid–base sites with higher strength due to the presence of MoO_3 on the support. Decanio *et al.* have also reported that when the Al_2O_3 is poisoned with a base the T_{max} of ethylene and diethylether desorption increases (62). Again, as in the case of the low-loading samples, the SiO_2 support is inert (Fig. 3c), as is known from the literature (67, 68). As the MoO_3 loading increases ethylene desorption is completely suppressed and a very small amount of diethylether is produced, indicating that the number of acid–base sites is reduced and the catalyst surface behaves almost like bulk MoO_3. On the high-loading SiO_2 sample, however, there is some formation of diethylether and ethylene along with acetaldehyde. This picture is completely consistent with our previous oxygen chemisorption, XRD, and laser Raman results. The interaction between the surface molybdenum oxide and the supports may be viewed as a generalized acid–base reaction. Under dehydrated conditions MoO_3 is weakly acidic, SiO_2 is slightly acidic, while Al_2O_3 and TiO_2 are amphoteric. Both *acidity* and *basicity* increase in the order $SiO_2 < Al_2O_3 \leq TiO_2$. The interaction of $MoO_3$with the supports thus increases in the order $SiO_2 < Al_2O_3 < TiO_2$, in agreement with earlier results (49, 68, 69).

Reactivity results are shown in Figs. 6 and 7. It should be stressed that our catalytic measurements are carried out in the presence of a controlled partial pressure of water vapor (10 kPa). Water is a side-product of oxidation which otherwise increases with conversion and could offset the kinetics of the reaction. The Arrhenius plots shown in Figs. 6 and 7 summarize the effect of support on steady-state catalytic activity for the low- and high-loading MoO_3 catalysts. In both cases, activity increases in the order $SiO_2 < Al_2O_3 < TiO_2$. In recent studies of methanol oxidation on various supported molybdenum and vanadium oxides the activity was also found to increase in the order $SiO_2 < Al_2O_3 < TiO_2$ (20, 71). The difference in activity has been attributed to the surface oxide–support interaction. The onset temperature of reduction for supported V_2O_5 (6, 70) and MoO_3 (72, 73) catalysts seemed to correlate with this activity difference. Similar trends in reactivity were found for ethanol oxidation on supported MoO_3 catalysts (74). In this study, Ono *et al.* attributed the difference in activity to the surface structures of the catalysts. We find that in propylene oxidation, the dependence of activity on support follows the same order as found in the alcohol oxidation reactions (72, 73). As presented earlier, this order corresponds to the strength of the metal oxide–support interaction, as indicated by Raman spectroscopy and the first reduction peak during temperature programmed reduction (Fig. 2).

However, there are also important differences. On the low-loading samples (Fig. 8) the predominant selective oxidation products were not the same: acrolein on MoO_3/SiO_2, acetaldehyde on MoO_3/Al_2O_3, and acetone on MoO_3/TiO_2. This indicates that the nature of the support–oxide interaction has a strong influence on the catalytic

chemistry of the active surface species. With an increase in loading, the degree of interaction is decreased and differences are reduced, so that acrolein is produced on all the samples. However, acetaldehyde is still produced on the Al_2O_3-supported sample while acetone is formed on the TiO_2-supported sample. As will be amplified below, we suggest that the acid–base nature of the interaction is responsible for directing the reaction to such different products.

There are few studies on the oxidation of propylene on MoO_3 supported on SiO_2 (14–16), Al_2O_3 (17, 18), and TiO_2 (19). Unfortunately it is difficult to compare our present work with that reported earlier due to the vast differences in conditions used. For example, some studies were done in the pulse mode (14, 17, 18) and some were done in the absence of water vapor (16, 19).

On the SiO_2-supported samples where the acid–base interactions between MoO_3 and SiO_2 are weak, the oxidation of propylene to acrolein probably occurs through a homolytic pathway involving the initial formation of allyl radicals. Such intermediates are well documented on bismuth molybdate catalysts (5).

On the Al_2O_3-supported samples with increasing acid–base interactions, the more polarizable portion of the molecule is activated, and it is likely that a π-complex is formed. As in the case of butene oxidative cleavage (75), this is followed by carbenium ion formation and scission of the molecule.

On the TiO_2-supported samples, again with strong acid–base interactions, activation of the double bond occurs, only this time to form isopropyl alcohol by hydration. This is then followed by dehydrogenation to acetone through an isopropoxy intermediate (76, 77). The mechanism is probably similar to that which occurs on Sn–Mo (24, 78). It has been shown in that system by using $H_2{}^{18}O$ tracer, that the oxygen atom in the ketone is incorporated from the water molecule and not from molecular oxygen (79).

It is clear that acid–base properties influence the products formed. This may be related fundamentally to the manner in which intermediates are bonded to the surface (80). Different intermediates are formed because on bonding to the surface the transition state derived from propylene is polarized in different manners depending on the acid–base environment it encounters.

In summary, oxygen chemisorption along with complementary evidence from XRD and laser Raman spectroscopy provides information on the nature of the MoO_3–support interaction. The interaction increases in the order $SiO_2 < Al_2O_3 < TiO_2$. The interaction of the MoO_3 with the support is of an acid–base nature. Temperature programmed desorption of ethanol from these samples indicate the presence of acid–base sites on the Al_2O_3- and TiO_2-supported samples. An increase in the MoO_3 loading tends to suppress these sites and characteristics of bulk MoO_3 start manifesting themselves in the samples. The low-loading and high-loading SiO_2 supported samples seem to be inert. The acidity and basicity of the supported samples increase in the same order as the MoO_3 support interaction. The activity for propylene oxidation increases in the order $SiO_2 < Al_2O_3 < TiO_2$ and correlates with the interaction of MoO_3 with the supports, the acid–base properties of the samples, and the initial temperature of reduction during temperature programmed reduction of these samples. Selectivity to partial oxidation products on the low-loading samples show major differences and is influenced by the acid–base characteristics of the surface and the nature of the reaction intermediate.

CONCLUSIONS

(i) The oxygen chemisorption technique indicates that the order of affinity of the supports for molybdenum oxide is $SiO_2 < Al_2O_3 < TiO_2$.

(ii) The interaction of the molybdenum oxide with the support is of an acid–base nature.

(iii) Ethanol temperature programmed desorption is an effective technique to probe the acid–base and oxidizing sites on the surfaces of these catalysts. TPD patterns indicate that both acidity and basicity increase in the order $SiO_2 < Al_2O_3 \leq TiO_2$.

(iv) The order for increase in activity for propylene oxidation is consistent with the MoO_3–support interaction, acid–base characteristics, and the reducibility of the catalysts.

ACKNOWLEDGMENTS

This work was supported by the National Science Foundation, Division of Chemical and Thermal Systems (CTS-9311876).

REFERENCES

1. Weissermel, K., and Arpe, H.-J., "Industrial Organic Chemistry." VCH, New York, 1993.
2. Adams, C. R., and Jennings, T. S., *J. Catal.* **2,** 63 (1963).
3. Krenze, J. D., and Keulks, G. W., *J. Catal.* **61,** 316 (1980).
4. Burrington, J. D., Kartisch, C. T., and Grasseli, R. K., *J. Catal.* **81,** 489 (1983).
5. Snyder, T. P., and Hill, Jr, C. G., *Catal. Rev. Sci. Eng.* **31,** 43 (1983).
6. Bond, G. C., Flamerz, S., and Shukri, R., *Faraday Discuss., Chem. Soc.* **87,** 65 (1989).
7. Zaki, M. I., Vielhabor, B., and Knozinger, H. J., *J. Phys. Chem.* **90,** 3176 (1986).
8. Nag, N. K., *J. Phys. Chem.* **91,** 2324 (1987).
9. Fransen, T., Mars, P., and Gellings, P. J., *J. Colloid Interface Sci.* **70,** 97 (1979).
10. Cáceres, C. V., Fierro, J. L. G., Lázaro, J., López Agudo, A., and Soria, J., *J. Catal.* **122,** 113 (1979).
11. Hattori, H., Tanabe, K., Tanaka, K., and Okazaki, S., *in* "Proceedings, 3rd International Conference on the Chemistry and Uses of Molybdenum." Climax Molybdenum Co., Ann Arbor, MI, 1979.
12. Muralidhar, G., Massoth, F. E., and Shabtai, J., *J. Catal.* **85,** 44 (1979).

13. Yang, J-T., and Lunsford, J., *J. Catal.* **103,** 55 (1987).
14. Vaghi, A., Castellan, A., Bart, J. C. J., Giordano, N., and Ragaini, V., *J. Catal.* **42,** 381 (1976).
15. Grabowski, R., Machej, T., Mazurkiewicz, A., and Sloczynski, J., *Bull. Pol. Acad. Sci.* 35 (1987).
16. Liu, T., Forissier, M., Coudurier, G., and Védrine, J., *J. Chem. Soc., Faraday, Trans. 1.* **85,** 1607 (1989).
17. Giordano, N., Padovan, M., Vaghi, A., Bart, J. C. J., and Castellan, A., *J. Catal.* **38,** 1 (1975).
18. Giordano, N., Vaghi, A., Bart, J. C. J., and Castellan, A., *J. Catal.* **38,** 11 (1975).
19. Ono, T., Nakagawa, Y., Miyata, H., and Kubokawa, Y., *Bull. Chem. Soc. Jpn.* **57,** 1205 (1984).
20. Matsuoka, Y., Niwa, M., and Murakami, Y., *J. Phys. Chem.* **94,** 1477 (1990).
21. Ashley, J. H., and Mitchell, P. C. H., *J. Chem. Soc.* **(A),** 2730 (1969).
22. Lipsch, J. M. J. G., and Schuit, G. C. A., *J. Catal.* **15,** 174 (1969).
23. Asmolov, G. N., and Krylov, O. V., *Kinet. Catal.* **11,** 847 (1970).
24. Giordano, N., Bart, J. C. J., Vaghi, A., Castellan, A., and Martinotti, G., *J. Catal.* **36,** 81 (1970).
25. Sonnemans, J., and Mars, P., *J. Catal.* **31,** 209 (1973).
26. Fransen, T., van der Meer, O., and Mars, P., *J. Catal.* **42,** 79 (1975).
27. Giordano, N., Bart, J. C. J., Castellan, A., and Vaghi, A., *J. Less-Common Met.* **54,** 387 (1977).
28. Seshadri, K. S., and Petrakis, L., *J. Phys. Chem.* **74,** 4102 (1977).
29. Dufaux, M., Che, M., and Naccache, C., *J. Chim. Phys.* **67,** 527 (1970).
30. Masson, J., Delmon, B., and Nachtschein, J., *C. R. Acad. Sci. Paris, Ser. C.* **266,** 1257 (1968).
31. Kasztelan, S., Payen, E., Toulhoat, H., Grimblot, J., and Bonnelle, J. P., *Polyhedron* **5,** 157 (1986).
32. Zingg, D. S., Makovsky, L. E., Tischer, R. E., Brown, F. R., and Hercules, D. M., *J. Phys. Chem.* **84,** 2898 (1980).
33. Brown, F. R., Makovsky, L. E., and Rhee, H. K., *J. Catal.* **50,** 162 (1977).
34. Knözinger, H., and Jeziorowski, H., *J. Phys. Chem.* **82,** 2002 (1978).
35. Jeziorowski, H., and Knözinger, H., *J. Phys. Chem.* **83,** 1166 (1979).
36. Williams, C. C., Ekerdt, J. G., Jehng, J.-M., Hardcastle, F. D., and Wachs, I. E., *J. Phys. Chem.* **95,** 8791 (1991).
37. Chan, S. S., Wachs, I. E., Murrell, L. L., Wang, L., and Hall, W. K., *J. Phys. Chem.* **88,** 5831 (1984).
38. Stencel, J. M., Makovsky, L. E., Sarkus, T. A., de Vries, J., Thomas, R., and Moulijn, J. A., *J. Catal.* **90,** 314 (1984).
39. Payen, E., Kasztelan, S., Grimblot, J., and Bonnelle, J. P., *J. Raman Spectrosc.* **30,** 233 (1986).
40. Kim, D. S., Segawa, K., Soeya, T., and Wachs, I. E., *J. Catal.* **136,** 539 (1992).
41. Datta, A. K., Ha, J-W., and Regalbuto, J. R., *J. Catal.* **133,** 55 (1992).
42. Kung, H. H., *Ind. Eng. Chem. Prod. Res. Dev.* **25,** 171 (1992).
43. Tanabe, K., "Solids Acids and Bases." Academic Press, New York, 1970.
44. Kijenski, J., and Baiker, A., *Catal. Today* **5,** 1 (1989).
45. Tanabe, K., Shibata, T., and Kitagawa, J., *Bull. Chem. Soc. Jpn.* **47,** 1064 (1974).
46. Jin, T., Hattori, H., and Tanabe, K., *Bull. Chem. Soc. Jpn.* **55,** 2279 (1982).
47. Gervasini, A., and Auroux, A., *J. Phys. Chem.* **97,** 2628 (1993).
48. Desikan, A. N., Huang, L., and Oyama, S. T., *J. Phys. Chem.* **95,** 10050 (1991).
49. Desikan, A. N., Huang, L., and Oyama, S. T., *J. Chem. Soc. Faraday Trans.* **88,** 3357 (1992).
50. Williams, C. C., Ekerdt, J. G., Jehng, J.-M., Hardcastle, F. D., and Wachs, I. E., *J. Phys. Chem.* **95,** 8781 (1991).
51. Farneth, W. R., Staley, R. H., and Sleight, A. W., *J. Phys. Chem.* **108,** 2327 (1986).
52. Padmanabhan, V. R., and Eastburn, F. J., *J. Catal.* **24,** 88 (1972).
53. Swabb, E. A., and Gates, B. C., *Ind. Eng. Chem. Fund.* **11** (1972).
54. Bandiera, J., and Naccache, C., *Appl. Catal.* **69,** 139 (1991).
55. Spivey, J. J., *Chem. Eng. Commun.* **110,** 123 (1991).
56. Tanabe, K., Misono, M., Ono, Y., and Hattori, H., *in* "New Solid Acids and Bases" (B. Delmon and J. T. Yates, Eds.), Vol. 51. Elsevier, Amsterdam, 1989.
57. Cunningham, J., Hodnett, B. K., Ilyas, M., Leahy, E. L., and Fierro, J. L. G., *Faraday Discuss. Chem. Soc.* **72,** 283 (1981).
58. Ai, M., *Bull. Chem. Soc. Jpn.* **50,** 2579 (1981).
59. Nollery, H., and Ritter, G. J., *Chem. Soc. Faraday Trans. 1* **80,** 275 (1984).
60. Ai, M., *J. Catal.* **40,** 318 (1975).
61. Ai, M., *J. Catal.* **40,** 327 (1975).
62. Decanio, E. C., Nero, V. P., and Bruno, J. W., *J. Catal.* **135,** 444 (1992).
63. Decanio, E. C., Bruno, J. W., Nero, V. P., and Edwards, J. C., *J. Catal.* **140,** 84 (1993).
64. Knözinger, H., Bühl, H., and Kochloefl, K., *J. Catal.* **24,** 57 (1972).
65. Peng, X. D., and Barteau, M., *Langmuir* **7,** 1426 (1991).
66. Figoli, N. S., Hillor, S. A., and Parera, J. M., *J. Catal.* **20,** 231 (1971).
67. Tanabe, K., *in* "Catalysis, Science and Technology" (J. R. Anderson and M. Boudart, Eds.), p. 231. Springer-Verlag, Berlin, 1981.
68. Auroux, A., and Gervasini, A., *J. Phys. Chem.* **94,** 6371 (1990).
69. Gervasini, A., and Auroux, A., *J. Catal.* **131,** 190 (1990).
70. Deo, G., and Wachs, I. E., *J. Catal.* **129,** 307 (1991).
71. Deo, G., and Wachs, I. E., *in* "Catalytic Selective Oxidation" (S. T. Oyama and J. Hightower, Eds.), ACS Symposium Series 523, p. 31. Am. Chem. Soc., Washington, DC, 1992.
72. Hu, H., and Wachs, I. E., *J. Phys. Chem.* **99,** 10911 (1995).
73. Hu, H., and Wachs, I. E., *J. Phys. Chem.* **99,** 10897 (1995).
74. Ono, T., Kamisuki, H., Hisashi, H., and Miyata, H., *J. Catal.* **116,** 303 (1989).
75. Takita, Y., Nita, K., Machara, T., Yamazol, N., and Seiyama, T., *J. Catal.* **50,** 364 (1977).
76. Buiten, J., *J. Catal.* **13,** 373 (1969).
77. Buiten, J., *J. Catal.* **27,** 232 (1972).
78. Takita, Y., Ozaki, A., and Moro-oka, Y., *J. Catal.* **27,** 185 (1972).
79. Moro-oka, Y., Takita, Y., and Ozaki, A., *J. Catal.* **27,** 177 (1972).
80. Oyama, S. T., Desikan, A. N., and Zhang, W., *in* "Catalytic Selective Oxidation" (S. T. Oyama and J. W. Hightower, Eds.), ACS Symposium Series 523, p. 16. Am. Chem. Soc., Washington, DC, 1993.